Journal of Applied Physics ARTICLE scitation.org/journal/jap

Rashba band splitting in two-dimensional Ruddlesden–Popper halide perovskites

Cite as: J. Appl. Phys. **128**, 175101 (2020); doi: 10.1063/5.0015965
Submitted: 2 June 2020 · Accepted: 4 October 2020 ·
Published Online: 2 November 2020

View Online Export Citation CrossMark

Shidong Yu,[1] Guangren Na,[1] Shulin Luo,[1] Oleg Rubel,[2] and Lijun Zhang[1,a)]

AFFILIATIONS

[1]State Key Laboratory of Integrated Optoelectronics, Key Laboratory of Automobile Materials of MOE and College of Materials Science and Engineering, Jilin University, Changchun 130012, China
[2]Department of Materials Science and Engineering, McMaster University, 1280 Main Street West, Hamilton, Ontario L8S 4L8, Canada

Note: This paper is part of the special collection on Hybrid Organic-Inorganic Halide Perovskites.
a)Author to whom correspondence should be addressed: lijun_zhang@jlu.edu.cn

ABSTRACT

Due to the presence of heavy elements and the dynamic nature of hybrid halide perovskites, the strong spin–orbit coupling effect can give rise to Rashba band splitting in these materials. Despite many reports on the Rashba effect in 3D perovskites like $CH_3NH_3PbI_3$, little is known about its presence in two-dimensional Ruddlesden–Popper (2DRP) perovskites. In this work, we use first-principle calculations to investigate the magnitude and origin of the Rashba effect in three families of 2DRP perovskites. We demonstrate the correlation between the splitting magnitude and the octahedron distortions. Moreover, different numbers of inorganic layers, spacer cations, and A-site cations have a great influence on the Rashba splitting through different mechanisms. While structures with $C_6H_5C_2H_4NH_3$ (PEA) have a significant Rashba splitting only in the monolayer condition, $C_4H_9NH_3$ (BA) induces large distortion by tilting the CH_3NH_3 (MA) cations around all octahedrons, giving rise to a larger Rashba splitting with an increasing number of inorganic layers. Our work elucidates the magnitude and origin of the Rashba splitting in 2DRP perovskites and provides guidelines for the manipulation of the Rashba splitting in these materials.

I. INTRODUCTION

Two-dimensional Ruddlesden–Popper (2DRP) perovskites have attracted great attention for their excellent ambient air stability compared with their 3D counterparts.[1–5] Their optoelectronic properties can be tuned by controlling their compositions and the number of inorganic layers, which make them promising candidates for optoelectronic applications.[4,6–8] Due to the presence of heavy elements like Pb, strong spin–orbit coupling is found in these hybrid materials. Combined with local electric fields caused by inversion symmetry breaking, the spin–orbit coupling (SOC) effect gives rise to Rashba band splitting.[9–12] The Rashba effect breaks the spin degeneracy at conduction and valence band edges and results in a quasi-indirect band structure,[9,13] as illustrated in Fig. 1(a). In solar cell applications, the strong Rashba effect in the absorber material may lead to low electron–hole recombination rate, long carrier lifetime, and therefore high power conversion efficiency (PCE) of the device.[9,13–15] However, the connection between the Rashba splitting and the long carrier lifetime remains controversial, as more detailed studies reveal no evidence for spin-forbidden optical transitions in perovskites.[16,17] Besides this, the Rashba effect also makes it possible to control and manipulate polarized spins in spintronic devices.[18]

Currently, the Rashba effect and its origin are well studied in 3D hybrid perovskites like $MAPbI_3$.[13,16,17,19–21] However, the Rashba effect in 2DRP perovskites is rarely studied. Experimentally, precessional spin relaxation is observed in $(BA)_2MAPb_2I_7$, which confirmed the presence of the Rashba effect.[22] Also, spin coherence lifetime is increased from 1.5 ps in the 3D case to 7 ps in $(BA)_2MA_3Pb_4I_{13}$, which indicates the potential influence of the Rashba effect.[23] Moreover, a giant Rashba splitting is obtained in PEA_2MAPbI_3 with a splitting energy of (40±5) meV.[24] Though Rashba splitting is observed experimentally in some 2DRP perovskites, it remains unclear how the structure parameters will influence the structural distortion and the splitting magnitude. The general formula of 2DRP perovskite is $(RNH_3)_2A_{n-1}M_nX_{3n+1}$ (n = 1, 2, 3, 4,…), where RNH_3 is a large

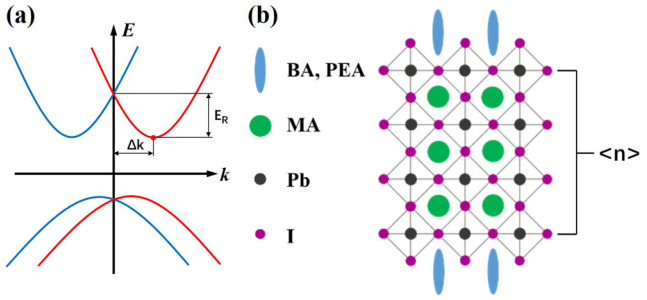

FIG. 1. (a) Schematic of the Rashba splitting with E_R as the splitting energy and Δk as the momentum offset. The two parabolic branches have the opposite spin. (b) Schematic of the structure of 2D Ruddlesden–Popper perovskites. Different components studied in this work are listed with their site. <n> indicates the number of inorganic layers.

aliphatic or aromatic alkylammonium spacer cation, A is a monovalent organic cation, M is a divalent metal cation, X is a halide anion, and n represents the number of MX_6 octahedron. In Fig. 1(b), we illustrate the structure of the 2DRP perovskites and the components studied in this work. The electronic properties of these materials change with different chemical components and the number of inorganic layers.[4,23,25] The origin of the Rashba effect in these materials is, therefore, more complicated. Hence, it remains a challenge for materials research to clarify the origin and mechanism of Rashba splitting in 2DRP perovskites.

In layered $MAPbI_3$, the structural distortion caused by different surface terminations is responsible for the observed Rashba effect, and the number of inorganic layers also has a prominent impact on the magnitude of Rashba splitting.[21,26,27] In both the 3D and layered $MAPbI_3$ systems, the Rashba effect is strongly related to the breaking of inversion symmetry in the structure, that is, the structural distortion, so we anticipate this is also valid in the 2DRP perovskite systems. However, there is not a unified definition of the structural distortion, and quantitative estimates of the Rashba splitting magnitude in 2DRP perovskites are hardly found.

In this work, via first-principle calculations, we explore the Rashba effect in three families of 2D Ruddlesden–Popper perovskites including $(BA)_2MA_{n-1}Pb_nI_{3n+1}$, $(PEA)_2MA_{n-1}Pb_nI_{3n+1}$, and $(PEA)_2Cs_{n-1}Pb_nI_{3n+1}$ (n = 1–6). Due to the influence of different spacer cations and A-site cations, their Rashba splitting magnitude changes in different patterns with increasing <n> value. Moreover, by investigating and comparing different structures, we aim to elucidate the origin and mechanism of Rashba band splitting in these materials. We demonstrate the correlation between the Rashba splitting magnitude and the distortion of the PbI_6 octahedron and explained how different components contribute to the distortion. Our results reveal the influence of different components and parameters on the magnitude of Rashba splitting and provide guidelines for the manipulation of Rashba splitting in 2DRP perovskites.

II. CALCULATION METHODS

The first-principle calculations were performed using plane-wave pseudopotential methods within the framework of density functional theory (DFT) as implemented in the Vienna *ab-initio* Simulation Package.[28,29] The electron–ion interaction was described using the frozen-core projected augmented-wave pseudopotentials.[30] The electron configurations of 1s for H, $2s^22p^2$ for C, $2s^22p^3$ for N, $5s^25p^5$ for I, $5s^25p^66s^1$ for Cs, and $6s^26p^2$ for Pb are considered valence electrons. The generalized gradient approximation formulated by Perdew *et al.*[31] was used as the exchange correlation functional (PBE functional). We used a kinetic energy cutoff of 400 eV for wave function expansion and a 4 × 4 × 1 Monkhorst-Pack k-point mesh for electronic Brillouin zone integration of 2D RP perovskites. The structures (including lattice parameters and internal atomic positions) were fully optimized via total energy minimization, with the total energy converged to less than 0.0001 eV. To properly take into account the long-range van der Waals (vdWs) interaction that is non-negligible for hybrid perovskites involving organic molecules, the vdWs optB86b functional is adopted.[32]

The original unit cell structures of tetragonal 2DRP perovskites are built with structural parameters a = b = 6.32 Å. The thickness of the vacuum layer is set as 30 Å to avoid the effect of interlayer interactions. In each family of 2DRP perovskites, the <n> = 6 structure is built and optimized first. MA cations in the inorganic layers are aligned with the X axis, with half of them in the opposite direction to cancel the dipole effect. This alignment is proved to have the lowest energy after testing several different alignments of MA cations. The <n> = 1–5 structures are built from the optimized <n> = 6 structure by removing inorganic layers from the center and optimized again. In order to clearly show the Rashba splitting, the K-path is selected in a small region in the Brillouin zone near the band edge. The k-points are selected as follows: L (0.5 0.5 0), Y′ (0.4 0.5 0), X′ (0.5 0.4 0), and Γ′ (0.4 0.4 0).

III. RESULTS AND DISCUSSION

A. Electronic structures of 2DRP perovskites

The electronic band structures of $(BA)_2MA_{n-1}Pb_nI_{3n+1}$ and $(PEA)_2MA_{n-1}Pb_nI_{3n+1}$ (<n> = 1–4) and the corresponding Rashba splitting energies at the conduction band edge are illustrated in Fig. 2. All band structures are calculated at the PBE + SOC + vdW level of theory. All structures have a quasi-direct band structure, with the parabolic band splitting near the *L* point in the Brillouin zone. A different magnitude of Rashba splitting is observed along different K paths, as is shown in the supplementary material. We use the largest one for discussion in this work for simplicity. In all structures, the magnitude of Rashba band splitting on the conduction band edge is significantly larger than that on the valence band edge. With increasing <n> value, the splitting energies of two families of 2DRP perovskites show different trends. The most prominent contrast happens in the <n> = 1 condition, where the $(BA)_2PbI_4$ structure shows almost no splitting while the largest splitting is observed in the $(PEA)_2PbI_4$ structure. As GGA functionals provide underestimated bandgap, we have also computed the band structures of PEA_2PbI_4 and $PEA_2MAPb_2I_7$ with the Heyd-Scuseria-Ernzerhof (HSE) hybrid functional.[33] The bandgap increased for ca. 0.51 eV, while the Rashba splitting energy has a little change (see Table S3 in the supplementary material).

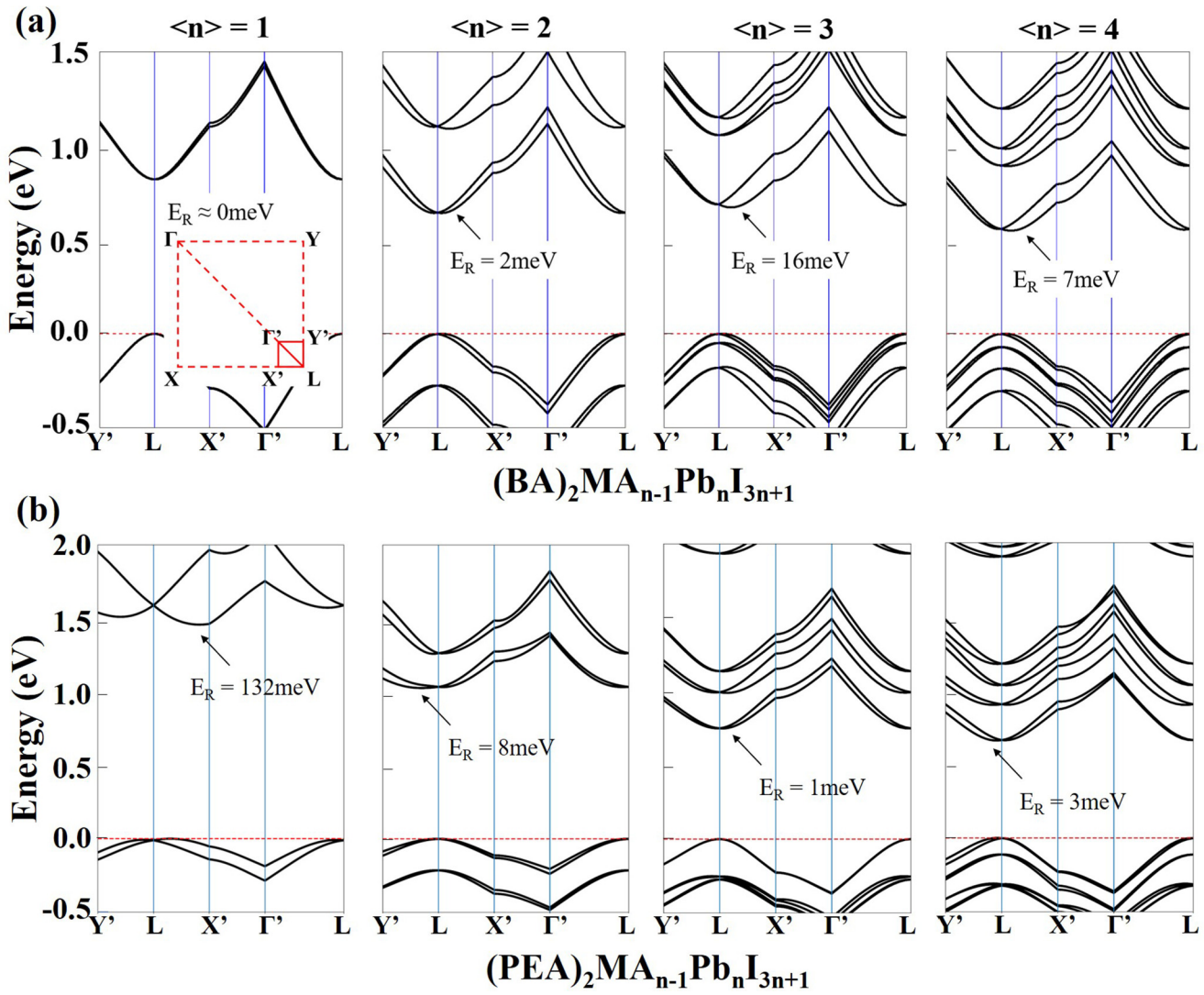

FIG. 2. Electronic band structures and the Rashba splitting energy at the conduction band of (a) $(BA)_2MA_{n-1}Pb_nI_{3n+1}$ and (b) $(PEA)_2MA_{n-1}Pb_nI_{3n+1}$ (<n> = 1–4). The inset on the left side of panel (a) shows the Brillouin zone and the k-points employed to calculate the band structure.

B. Rashba splitting magnitude of 2DRP perovskites

To clearly demonstrate the magnitude of the Rashba splitting, we use the splitting energy E_R and the Rashba coefficient α_R as parameters. The Rashba coefficient is calculated as

$$\alpha_R = \frac{2E_R}{\Delta k}. \quad (1)$$

The Rashba parameters of $(BA)_2MA_{n-1}Pb_nI_{3n+1}$ and $(PEA)_2MA_{n-1}Pb_nI_{3n+1}$ (<n> = 1–6) are shown in Fig. 3. By comparing these two families of 2DRP perovskites, we can see the different impact of BA and PEA cations on the Rashba splitting. Both the splitting energy and the Rashba coefficient are much more prominent in the conduction band than in the valence band. This is possibly due to the different density of states at the conduction and valence band edges. The Rashba splitting arises from the spin–orbit coupling effect, which is dependent on the total angular momentum ***J*** of the electrons. Therefore, the p-electrons will experience a larger shift in the energy level than the s-electrons. According to our results, the VBM of the hybrid perovskites mainly consists of the 5p of I and a large portion of the 6s of Pb, while the CBM mainly consists of Pb 6p. Therefore, the Rashba splitting energy and coefficient at the conduction band is expected to be much larger than that of the valence band. In this work, we will mainly study the magnitude of Rashba splitting in the

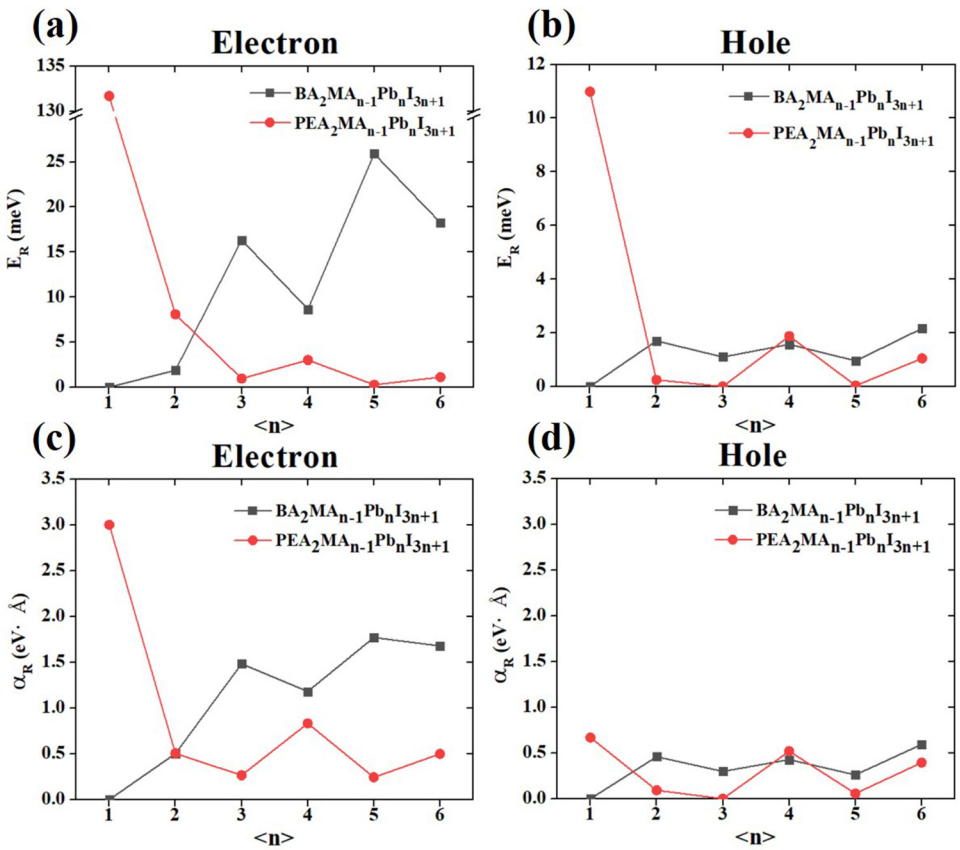

FIG. 3. Calculated (a) and (b) Rashba splitting energy and (c) and (d) coefficient of $(BA)_2MA_{n-1}Pb_nI_{3n+1}$ and $(PEA)_2MA_{n-1}Pb_nI_{3n+1}$ (<n> = 1–6) at the conduction and valence band edges.

conduction band. In the $(BA)_2MA_{n-1}Pb_nI_{3n+1}$ family, almost no splitting is observed at <n> = 1 condition, but the magnitude of Rashba splitting increases with increasing <n> in a general trend. The E_R at the conduction band reaches a maximum of 26 meV at <n> = 5. On the other hand, in the $(PEA)_2MA_{n-1}Pb_nI_{3n+1}$ family, a significant Rashba splitting is observed at <n> = 1 condition, but it quickly decreases with increasing <n>, with E_R at the conduction band less than 5 meV at <n> = 3–6. Specifically, in the <n> = 2–6 condition, the parity of the <n> value has an influence on the Rashba splitting. In the $(BA)_2MA_{n-1}Pb_nI_{3n+1}$ family, structures with odd <n> value have larger Rashba than those with even <n> value. While in the $(PEA)_2MA_{n-1}Pb_nI_{3n+1}$ family, the condition is the opposite. The previous work also suggests that intrinsic Rashba splitting only exists in structures with an even <n> value, but not for the ones with an odd <n> value.[26]

To further investigate the influence of A-site cations on the Rashba splitting, we replaced the MA cations with Cs cations and fully relaxed the atomic positions and lattice parameters as described in Sec. II. The calculated Rashba splitting magnitudes in the $(PEA)_2Cs_{n-1}Pb_nI_{3n+1}$ family are shown in Fig. 4. In general, the splitting magnitude of the $(PEA)_2Cs_{n-1}Pb_nI_{3n+1}$ family is very similar to the $(PEA)_2MA_{n-1}Pb_nI_{3n+1}$ family. After the Cs replacement, the splitting energy does not fluctuate with increasing <n> but decreases continuously. In the <n> = 3–6 condition, the splitting energy at both the conduction and valence bands is below 1 meV. This indicates that MA cations might be the cause for the correlation between the splitting magnitude and the parity of the <n> value.

C. Structural distortion and its origin

Next, we investigate the distortion of PbI_6 octahedrons and its origin, in order to explain the different splitting magnitude in different structures. We use Δθ to represent the distortion of PbI_6 octahedrons. In each octahedron, Δθ is defined as the following equation:

$$\Delta\theta = \frac{\sum_{i=1}^{3}(180 - \theta_i)}{3}, \tag{2}$$

as is depicted in Fig. 5(a). In a 2DRP perovskite structure, Δθ indicates the average distortion of all octahedrons calculated with the same method. To resolve an ambiguity in the definition of the angle θ_i associated with 2π wrapping, we always selected a value less than 180°. From the distortions of each 2DRP perovskite in Fig. 5(b), we can see that the distortion generally has the same

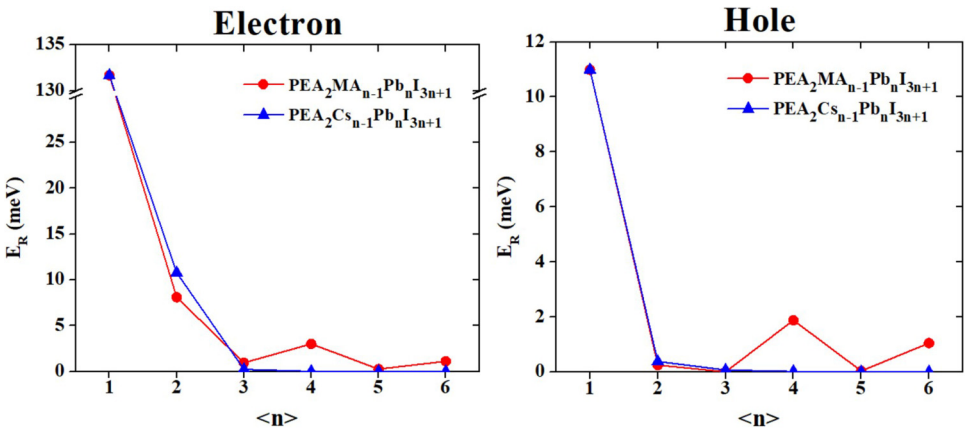

FIG. 4. Calculated Rashba splitting energies for $(PEA)_2MA_{n-1}Pb_nI_{3n+1}$ and $(PEA)_2Cs_{n-1}Pb_nI_{3n+1}$ (<n> = 1–6) at the conduction and valence band edges. (Upon Cs substitution, the lattice parameters and all atomic positions were relaxed.)

trend with the Rashba parameters, large distortion leads to a large Rashba splitting (see Fig. S1 in the supplementary material). In the <n> = 1 condition, PEA cation causes large distortion and therefore large Rashba splitting, while BA leads to very little distortion and almost no Rashba splitting. With increasing <n>, the influence of spacer cations becomes less dominant, and the distortion of the Pb–I cage is mainly induced by their interaction with the MA cations around them.

In Figs. 5(c)–5(e), we can see that BA cation causes the tilting of all MA cations inside the structure through vdW interaction. While in the $(PEA)_2MA_{n-1}Pb_nI_{3n+1}$ family, MA cations inside the inorganic layer mostly remain parallel to the 2D plane.

By calculating the dipole moment of BA and PEA, we found that BA has a dipole moment of 1.094 e Å in the Z direction, which is much larger than the 0.413 e Å dipole moment of PEA. Also, as is shown in Figs. 5(c)–5(e), the amino group at the end of PEA is perpendicular to the X–Y plane, while the amino group at the end of BA is not. This results in a large dipole moment of 0.701 e Å from BA along the X direction. Therefore, due to the larger dipole of BA and its tilted direction, it is much easier for BA to induce the tilting of MA cations than PEA. Also, in the $(BA)_2MA_{n-1}Pb_nI_{3n+1}$ family, every octahedron has large distortion, while in the $(PEA)_2MA_{n-1}Pb_nI_{3n+1}$ and $(PEA)_2Cs_{n-1}Pb_nI_{3n+1}$ family, only octahedrons near the PEA cations have large distortion. This indicates that the orientation of the MA cations has a great influence on the distortion of the PbI_6 octahedron around them. On the other hand, almost no distortion is observed in the octahedrons in the center of the $(PEA)_2Cs_5Pb_6I_{19}$ structure, possibly due to the stabilization effect of Cs atoms.[34–36] The lack of distortion inside the structure explains the decrease of Rashba splitting magnitude with increasing <n> in the two families of 2DRP perovskites with PEA cations. We notice that all structures in this work are simulated in a static situation due to computation cost. Considering the soft nature of the Pb–I framework, we anticipate the fluctuation of the distortion of the Pb–I framework and the magnitude of the Rashba splitting in time.[13,17,19]

The relationship between the parity of <n> and the Rashba effect originates in the relationship between the parity of the number of MA cation layers and the Rashba effect. When the number of MA cation layers changes, the overall condition of the MA cations orientation also changes when the structure is relaxed. This, in turn, influences the distortion of the PbI_6 octahedrons and the local dipole field around them, which gives different Rashba splitting magnitudes. As is shown in Figs. 5(b) and 6(b), $(BA)_2MA_{n-1}Pb_nI_{3n+1}$ structures with an even value of <n> have slightly smaller distortion and much weaker E_Z, which leads to a smaller Rashba splitting magnitude. To further testify the influence of the MA cations, we replace MA with Cs in the structures of the $(BA)_2MA_{n-1}Pb_nI_{3n+1}$ family *without* relaxing the Pb–I cages, in order to cancel the dipole field of MA cations. The result suggests that the correlation between the splitting magnitude and the parity of the <n> value vanished (see Fig. S2 in the supplementary material). The results of the splitting energy at the conduction band are provided in the supplementary material.

D. Local electrostatic field

Although different models of the Rashba effect in hybrid halide perovskites are proposed,[9,16,36] the magnitude of the Rashba splitting is in principle related to the local electrostatic field perpendicular to the sample plane. Therefore, we calculated the electrostatic potential in each 2DRP perovskite and the gradient of electrostatic potential along the Z direction as the electric field E_Z. The electric field around each octahedron is contributed by both the distortion of the Pb–I cage and the cations around it. The strength of the electric field has similar trends with the magnitude of the Rashba splitting (see Fig. S3 in the supplementary material), and the correlation between the strength of the electric field and the parity of the <n> value is also present in the $(BA)_2MA_{n-1}Pb_nI_{3n+1}$ family, which can be a result of the residual dipole field of the MA cations. While the octahedron distortion being the major cause for the Rashba splitting, the influence of the local electric field is also non-negligible.

E. MA cation orientations

To further investigate the relationship between MA cation orientation and the Rashba splitting, we calculated the relaxed atomic structures and band structures of $(PEA)_2MA_{n-1}Pb_nI_{3n+1}$

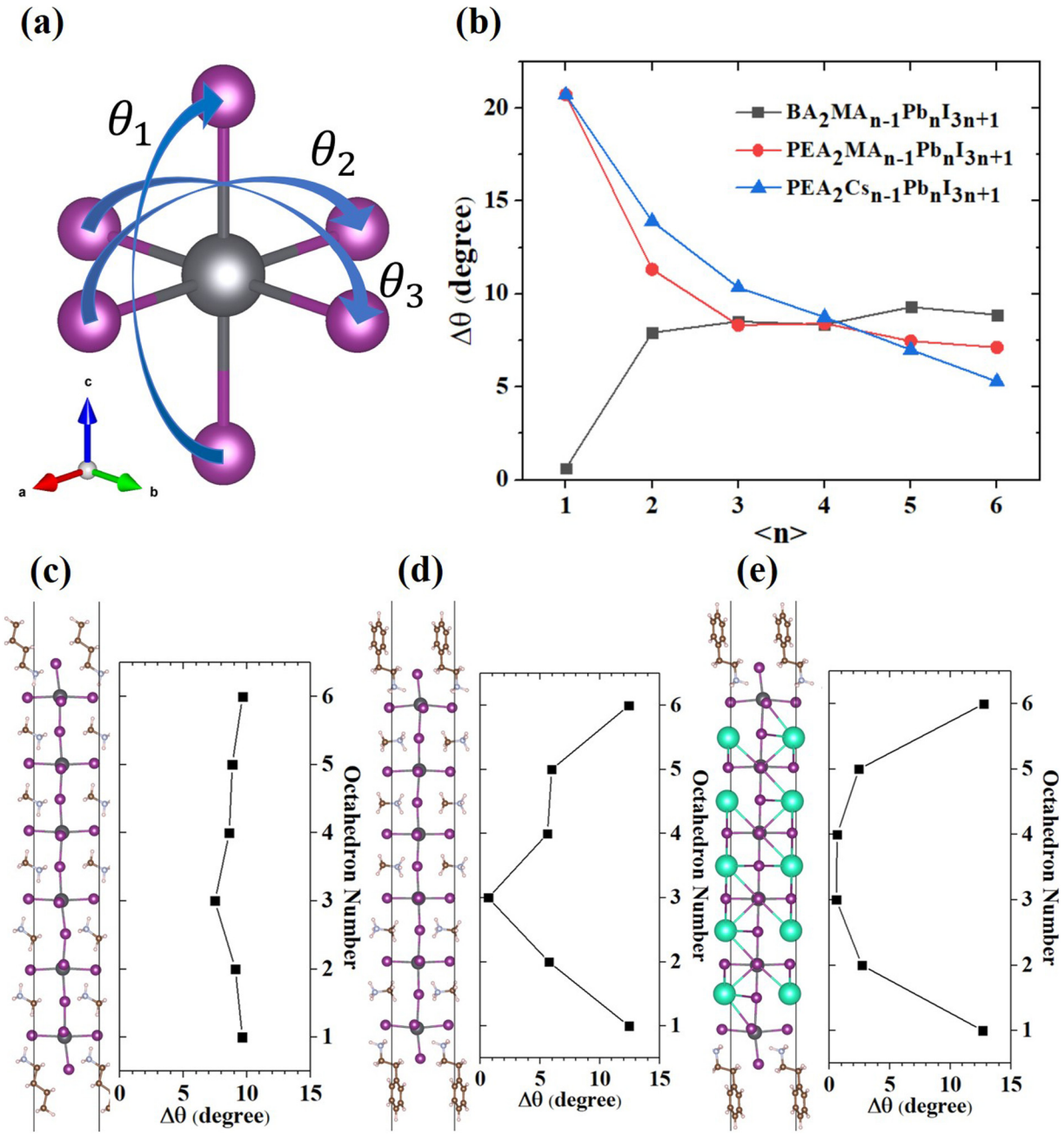

FIG. 5. (a) Three I–Pb–I angles in a PbI_6 octahedron. (b) The octahedron distortion in three families of 2DRP perovskites. The atomic structure of (c) $BA_2MA_5Pb_6I_{19}$, (d) $PEA_2MA_5Pb_6I_{19}$, and (e) $PEA_2Cs_5Pb_6I_{19}$ and the corresponding distortion of each PbI_6 octahedron. (Upon Cs substitution, the lattice parameters and all atomic positions were relaxed.)

(<n> = 1–6) with all the MA cations oriented vertically to the X–Y plane. As is shown in Fig. 7, for structures with <n> = 2–6, the splitting energy is significantly larger when the MA cations are vertically oriented. In the structures with vertically oriented MA cations, the splitting energy decreased for <n> = 1–3 due to the fading influence from the PEA cations. However, the splitting energy increased for <n> = 3–6, which is different from the parallel-oriented structures. We believe this is due to the

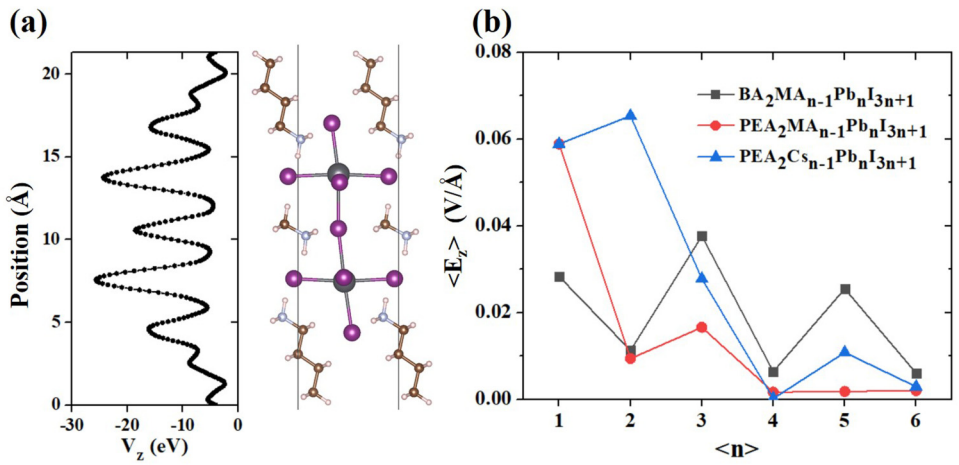

FIG. 6. (a) Computed potential profile of $BA_2MAPb_2I_7$ and its atomic structure. (b) The average E_Z in each inorganic layer in different 2DRP perovskites. The electric field E_Z is calculated as the gradient of electrostatic potential along the Z direction. (Upon Cs substitution, the Pb–I cage, lattice parameters, and positions of Cs atoms were relaxed.)

accumulation of the dipole field from the MA cations with aligned orientation. As the number of MA cations increased with <n>, the Rashba splitting energy increases with the strengthening dipole field vertical to the X–Y plane. It should be noted that the structures with vertically oriented MA cations have higher energy than that with parallel orientations. For the <n> = 6 structures in Fig. 7(a), the energy of the "vertical" structure is higher than the "parallel" structure by 220 meV per formula unit, similar to previous findings in $MAPbI_3$.[37] By comparing these two groups, we can see that the MA cation orientation in the structure has a great influence on the Rashba splitting magnitude when their dipole field is accumulated, but it also results in a metastable state of the structure.

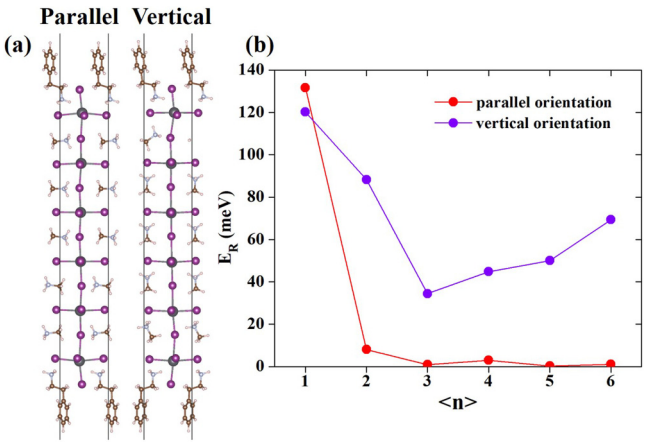

FIG. 7. (a) The atomic structures of $PEA_2MA_5Pb_6I_{19}$ with parallel and vertical MA cation orientations. (b) Rashba splitting energy at the conduction band of $(PEA)_2MA_{n-1}Pb_nI_{3n+1}$ (<n> = 1–6) structures with parallel and vertical MA cation orientations.

IV. CONCLUSION

In this work, we investigated the magnitude and origin of the Rashba splitting in three families of two-dimensional Ruddlesden–Popper perovskites by first-principle calculations. The spin–orbit coupling effect and the van der Waals interactions are included. Our results show that the Rashba splitting is related to the distortion of the PbI_6 octahedron. In structures with PEA, a significant Rashba splitting is only observed in the small <n> condition as a result of large distortion at the organic–inorganic interface. On the other hand, the splitting magnitude of structures with BA and MA increases with <n>, as a consequence of the tilted orientation of MA induced by BA. Moreover, unlike dipole cations like MA, cations tend to stabilize the octahedrons as the A-site cation and lead to lower splitting magnitude. Our study suggests that the selection of chemical components and the number of inorganic layers have a great influence on the magnitude of the Rashba splitting in two-dimensional Ruddlesden–Popper perovskites. The results of this work provide guidelines for the manipulation of Rashba splitting magnitude in two-dimensional Ruddlesden–Popper perovskites through chemical structure design.

SUPPLEMENTARY MATERIAL

See the supplementary material for the structural data of the lowest energy structures of $(BA)_2MA_5Pb_6I_{19}$, $(PEA)_2MA_5Pb_6I_{19}$, and $(PEA)_2Cs_5Pb_6I_{19}$, the splitting energy after the replacement of MA with Cs, the splitting energy along different directions in the Brillouin zone, the splitting energies for PEA_2PbI_4 and $PEA_2MAPb_2I_7$ calculated with HSE06 functional, the correlation between the splitting energy and the distortion, and the correlation between the splitting energy and the average electric field.

ACKNOWLEDGMENTS

This work is supported by the National Natural Science Foundation of China (Grant Nos. 61722403 and 11674121) and Jilin Province Science and Technology Development Program

(Grant No. 20190201016JC). Calculations were performed in part at the high-performance computing center of Jilin University. S.Y. would like to acknowledge funding from Mitacs via Globalink program that supported his internship at McMaster University.

DATA AVAILABILITY

The data that support the findings of this study are available within the article and its supplementary material.

REFERENCES

[1]I. C. Smith, E. T. Hoke, D. Solis-Ibarra, M. D. McGehee, and H. I. Karunadasa, Angew. Chem. Int. Ed. **53**, 11232 (2014).
[2]D. H. Cao, C. C. Stoumpos, O. K. Farha, J. T. Hupp, and M. G. Kanatzidis, J. Am. Chem. Soc. **137**, 7843 (2015).
[3]H. Tsai, W. Nie, J.-C. Blancon, C. C. Stoumpos, R. Asadpour, B. Harutyunyan, A. J. Neukirch, R. Verduzco, J. J. Crochet, S. Tretiak, L. Pedesseau, J. Even, M. A. Alam, G. Gupta, J. Lou, P. M. Ajayan, M. J. Bedzyk, M. G. Kanatzidis, and A. D. Mohite, Nature **536**, 312 (2016).
[4]Y. Chen, Y. Sun, J. Peng, J. Tang, K. Zheng, and Z. Liang, Adv. Mater. **30**, 1703487 (2018).
[5]L. N. Quan, M. Yuan, R. Comin, O. Voznyy, E. M. Beauregard, S. Hoogland, A. Buin, A. R. Kirmani, K. Zhao, A. Amassian, D. H. Kim, and E. H. Sargent, J. Am. Chem. Soc. **138**, 2649 (2016).
[6]C. C. Stoumpos, D. H. Cao, D. J. Clark, J. Young, J. M. Rondinelli, J. I. Jang, J. T. Hupp, and M. G. Kanatzidis, Chem. Mater. **28**, 2852 (2016).
[7]R. Quintero-Bermudez, A. Gold-Parker, A. H. Proppe, R. Munir, Z. Yang, S. O. Kelley, A. Amassian, M. F. Toney, and E. H. Sargent, Nat. Mater. **17**, 900 (2018).
[8]Z. Liu, G. Na, F. Tian, L. Yu, J. Li, and L. Zhang, InfoMat **2**, 879 (2020).
[9]F. Zheng, L. Z. Tan, S. Liu, and A. M. Rappe, Nano Lett. **15**, 7794 (2015).
[10]A. Manchon, H. C. Koo, J. Nitta, S. M. Frolov, and R. A. Duine, Nat. Mater. **14**, 871 (2015).
[11]M. Kim, J. Im, A. J. Freeman, J. Ihm, and H. Jin, Proc. Natl. Acad. Sci. U.S.A. **111**, 6900 (2014).
[12]M. Kepenekian, R. Robles, C. Katan, D. Sapori, L. Pedesseau, and J. Even, ACS Nano **9**, 11557 (2015).
[13]T. Etienne, E. Mosconi, and F. De Angelis, J. Phys. Chem. Lett. **7**, 1638 (2016).
[14]E. M. Hutter, M. C. Gélvez-Rueda, A. Osherov, V. Bulović, F. C. Grozema, S. D. Stranks, and T. J. Savenije, Nat. Mater. **16**, 115 (2017).
[15]P. Azarhoosh, S. McKechnie, J. M. Frost, A. Walsh, and M. van Schilfgaarde, APL Mater. **4**, 091501 (2016).
[16]X. Zhang, J.-X. Shen, and C. G. Van de Walle, J. Phys. Chem. Lett. **9**, 2903 (2018).
[17]C. Zheng, S. Yu, and O. Rubel, Phys. Rev. Mater. **2**, 114604 (2018).
[18]M. Kepenekian and J. Even, J. Phys. Chem. Lett. **8**, 3362 (2017).
[19]T. Etienne, E. Mosconi, and F. De Angelis, J. Phys. Chem. C **122**, 124 (2018).
[20]Z.-G. Yu, J. Phys. Chem. C **122**, 29607 (2018).
[21]E. Mosconi, T. Etienne, and F. De Angelis, J. Phys. Chem. Lett. **8**, 2247 (2017).
[22]S. B. Todd, D. B. Riley, A. Binai-Motlagh, C. Clegg, A. Ramachandran, S. A. March, I. G. Hill, M. G. Kanatzidis, Z.-G. Yu, and K. C. Hall, APL Mater. **7**, 081116 (2019).
[23]X. Chen, H. Lu, Z. Li, Y. Zhai, P. F. Ndione, J. J. Berry, K. Zhu, Y. Yang, and M. C. Beard, ACS Energy Lett. **3**, 2273 (2018).
[24]Y. Zhai, S. Baniya, C. Zhang, J. Li, P. Haney, C.-X. Sheng, E. Ehrenfreund, and Z. V. Vardeny, Sci. Adv. **3**, e1700704 (2017).
[25]J. Hu, L. Yan, and W. You, Adv. Mater. **30**, 1802041 (2018).
[26]J. Yin, P. Maity, L. Xu, A. M. El-Zohry, H. Li, O. M. Bakr, J.-L. Brédas, and O. F. Mohammed, Chem. Mater. **30**, 8538 (2018).
[27]C. W. Myung, S. Javaid, K. S. Kim, and G. Lee, ACS Energy Lett. **3**, 1294 (2018).
[28]G. Kresse and J. Furthmüller, Phys. Rev. B **54**, 11169 (1996).
[29]G. Kresse and J. Furthmüller, Comput. Mater. Sci. **6**, 15 (1996).
[30]P. E. Blöchl, Phys. Rev. B **50**, 17953 (1994).
[31]J. P. Perdew, K. Burke, and M. Ernzerhof, Phys. Rev. Lett. **77**, 3865 (1996).
[32]J. Klimeš, D. R. Bowler, and A. Michaelides, Phys. Rev. B **83**, 195131 (2011).
[33]J. Heyd, G. E. Scuseria, and M. Ernzerhof, J. Chem. Phys. **118**, 8207–8215 (2003).
[34]M. Saliba, T. Matsui, J.-Y. Seo, K. Domanski, J.-P. Correa-Baena, M. K. Nazeeruddin, S. M. Zakeeruddin, W. Tress, A. Abate, A. Hagfeldt, and M. Grätzel, Energy Environ. Sci. **9**, 1989 (2016).
[35]X. Jia, C. Zuo, S. Tao, K. Sun, Y. Zhao, S. Yang, M. Cheng, M. Wang, Y. Yuan, J. Yang, F. Gao, G. Xing, Z. Wei, L. Zhang, H.-L. Yip, M. Liu, Q. Shen, L. Yin, L. Han, S. Liu, L. Wang, J. Luo, H. Tan, Z. Jin, and L. Ding, Sci. Bull. **64**, 1532 (2019).
[36]Z.-G. Yu, J. Phys. Chem. Lett. **7**, 3078 (2016).
[37]Q. Xu, A. Stroppa, J. Lv, X. Zhao, D. Yang, K. Biswas, and L. Zhang, Phys. Rev. Mater. **3**, 125401 (2019).

Supplementary Material

Rashba Band Splitting in Two-dimensional Ruddlesden-Popper Halide Perovskites

Shidong Yu[1], Guangren Na[1], Shulin Luo[1], Oleg Rubel[2], Lijun Zhang[1,a)]

AFFILIATIONS

[1]State Key Laboratory of Integrated Optoelectronics, Key Laboratory of Automobile Materials of MOE and College of Materials Science and Engineering, Jilin University, Changchun 130012, China

[2]Department of Materials Science and Engineering, McMaster University, 1280 Main Street West, Hamilton, Ontario L8S 4L8, Canada

[a)]Author to whom correspondence should be addressed: lijun_zhang@jlu.edu.cn

Table S1 Structural data of the lowest-energy structures of $(BA)_2MA_5Pb_6I_{19}$, $(PEA)_2MA_5Pb_6I_{19}$ and $(PEA)_2Cs_5Pb_6I_{19}$. The fractional coordinates of all atoms except H are given**.** (Upon Cs substitution, the lattice parameters as well as all atomic positions were relaxed.)

Material Space group	Lattice parameters(Å)	Wyckoff positions	Atoms	x	y	z	Atoms	x	y	z
$(BA)_2MA_5Pb_6I_{19}$ P1	a=6.21891	1a	C1	0.99706	0.9348	0.3333	I11	0.4124	0.9360	0.6205
	b=6.15127		C2	0.99514	0.9402	0.4127	I12	0.4141	0.9341	0.7030
	c=77.73251		C3	0.8674	0.9420	0.5052	I13	0.5342	0.4334	0.2525
	α=90°		C4	0.8730	0.9353	0.5864	I14	0.4735	0.4349	0.3355
	β=90°		C5	0.8703	0.9339	0.6678	I15	0.4834	0.4410	0.4183
	γ=90°		C6	0.1987	0.9326	0.2243	I16	0.3966	0.4436	0.5005
			C7	0.9951	0.9327	0.2353	I17	0.3997	0.4380	0.5831
			C8	0.0476	0.9335	0.2545	I18	0.3944	0.4343	0.6658
			C9	0.1470	0.9313	0.2051	I19	0.3358	0.4337	0.7489
			C10	0.6722	0.9331	0.7772	N1	0.7843	0.9349	0.3423
			C11	0.8755	0.9330	0.7661	N2	0.8003	0.9392	0.4241
			C12	0.8225	0.9339	0.7470	N3	0.0811	0.9441	0.4964
			C13	0.7244	0.9318	0.7964	N4	0.0848	0.9385	0.5774
			I1	0.9691	0.4341	0.2940	N5	0.0832	0.9343	0.6589
			I2	0.9461	0.4391	0.3741	N6	0.8437	0.9336	0.2648
			I3	0.9161	0.4644	0.4611	N7	0.0260	0.9339	0.7366
			I4	0.9247	0.4430	0.5446	Pb1	0.4685	0.4342	0.2926

			I5	0.9245	0.4353	0.6270	Pb2	0.4419	0.4386	0.3761
			I6	0.9000	0.4339	0.7074	Pb3	0.4202	0.4507	0.4592
			I7	0.4545	0.9343	0.2984	Pb4	0.4297	0.4416	0.5425
			I8	0.4549	0.9389	0.3807	Pb5	0.4294	0.4358	0.6253
			I9	0.3834	0.9515	0.4566	Pb6	0.4007	0.4340	0.7088
			I10	0.4077	0.9419	0.5385				
$(PEA)_2MA_5Pb_6I_{19}$	a=6.23527	1a	C1	0.9194	0.9693	0.3454	I7	0.3978	0.9010	0.3024
P1	b=6.24101		C2	0.9294	0.9948	0.4201	I8	0.4266	0.9244	0.3817
	c=79.61593		C3	0.9228	0.8577	0.5015	I9	0.4265	0.9264	0.4604
	α=90°		C4	0.9176	0.8502	0.5786	I10	0.4111	0.9217	0.5404
	β=90°		C5	0.9286	0.8930	0.6548	I11	0.4208	0.9328	0.6180
	γ=90°		C6	0.0183	0.0686	0.1981	I12	0.4035	0.9599	0.6977
			C7	0.8270	0.1408	0.2053	I13	0.4246	0.4545	0.2606
			C8	0.8025	0.1429	0.2227	I14	0.4207	0.4293	0.3405
			C9	0.9694	0.0739	0.2332	I15	0.4137	0.4461	0.4205
			C10	0.1615	0.0029	0.2259	I16	0.4394	0.4054	0.5000
			C11	0.1858	0.9995	0.2085	I17	0.4369	0.4045	0.5795
			C12	0.9421	0.0670	0.2520	I18	0.4282	0.4320	0.6595
			C13	0.9138	0.8359	0.2577	I19	0.4358	0.4073	0.7395
			C14	0.0420	0.7937	0.8018	N1	0.9161	0.7315	0.3431
			C15	0.8503	0.7198	0.7948	N2	0.8986	0.7590	0.4222
			C16	0.8234	0.7175	0.7773	N3	0.9549	0.0933	0.4993

			C17	0.9883	0.7880	0.7667	N4	0.9544	0.0867	0.5783
			C18	0.1807	0.8608	0.7739	N5	0.9358	0.1308	0.6570
			C19	0.2074	0.8642	0.7913	N6	0.8974	0.8232	0.2765
			C20	0.9581	0.7950	0.7479	N7	0.9032	0.0385	0.7236
			C21	0.9218	0.0254	0.7424	Pb1	0.4109	0.4023	0.2984
			I1	0.9102	0.3601	0.3027	Pb2	0.4291	0.4200	0.3802
			I2	0.9295	0.4435	0.3823	Pb3	0.4258	0.4263	0.4602
			I3	0.9260	0.4272	0.4606	Pb4	0.4184	0.4277	0.5399
			I4	0.9174	0.3951	0.5390	Pb5	0.4200	0.4377	0.6197
			I5	0.9196	0.4148	0.6178	Pb6	0.4139	0.4587	0.7016
			I6	0.9131	0.5008	0.6973				
$(PEA)_2Cs_5Pb_6I_{19}$	a=6.22743	1a	C1	0.0128	0.0656	0.2001	I9	0.4305	0.9251	0.4607
P1	b=6.23827		C2	0.8202	0.1301	0.2075	I10	0.4317	0.9410	0.5394
	c=71.61593		C3	0.7962	0.1228	0.2250	I11	0.4337	0.9606	0.6179
	α=90°		C4	0.9653	0.0523	0.2352	I12	0.4145	0.9968	0.6960
	β=90°		C5	0.1586	0.9888	0.2276	I13	0.4218	0.4251	0.2624
	γ=90°		C6	0.1823	0.9948	0.2102	I14	0.4189	0.3932	0.3419
			C7	0.9391	0.0357	0.2540	I15	0.4285	0.4144	0.4211
			C8	0.9133	0.8015	0.2589	I16	0.4310	0.4330	0.5000
			C9	0.0372	0.7963	0.7998	I17	0.4318	0.4512	0.5790
			C10	0.8443	0.7308	0.7924	I18	0.4279	0.4714	0.6582
			C11	0.8192	0.7382	0.7750	I19	0.4397	0.4369	0.7377

	C12	0.9871	0.8098	0.7647	N1	0.9006	0.7785	0.2777
	C13	0.1806	0.8743	0.7722	N2	0.9148	0.0837	0.7223
	C14	0.2056	0.8681	0.7896	Pb1	0.4100	0.3677	0.3004
	C15	0.9594	0.8265	0.7460	Pb2	0.4271	0.4050	0.3810
	C16	0.9294	0.0604	0.7410	Pb3	0.4303	0.4251	0.4605
	I1	0.9094	0.3160	0.3049	Pb4	0.4316	0.4410	0.5397
	I2	0.9272	0.4045	0.3822	Pb5	0.4320	0.4609	0.6191
	I3	0.9303	0.4258	0.4607	Pb6	0.4232	0.4951	0.6997
	I4	0.9316	0.4404	0.5394	Cs1	0.9366	0.9631	0.6536
	I5	0.9321	0.4619	0.6179	Cs2	0.9316	0.9440	0.5776
	I6	0.9222	0.5461	0.6951	Cs3	0.9338	0.9342	0.5000
	I7	0.4008	0.8661	0.3040	Cs4	0.9301	0.9211	0.4224
	I8	0.4295	0.9053	0.3823	Cs5	0.9325	0.9038	0.3467

Table S2 Rashba splitting energy at the conduction band of $(BA)_2MA_{n-1}Pb_nI_{3n+1}$, $(PEA)_2MA_{n-1}Pb_nI_{3n+1}$, and $(PEA)_2Cs_{n-1}Pb_nI_{3n+1}$ (<n>=1~6) along the directions $L\rightarrow X$, $L\rightarrow \Gamma$ and $L\rightarrow Y$. (Upon Cs substitution, the lattice parameters as well as all atomic positions were relaxed.)

	E_R (meV)								
	$(BA)_2MA_{n-1}Pb_nI_{3n+1}$			$(PEA)_2MA_{n-1}Pb_nI_{3n+1}$			$(PEA)_2Cs_{n-1}Pb_nI_{3n+1}$		
	$L\rightarrow X$	$L\rightarrow \Gamma$	$L\rightarrow Y$	$L\rightarrow X$	$L\rightarrow \Gamma$	$L\rightarrow Y$	$L\rightarrow X$	$L\rightarrow \Gamma$	$L\rightarrow Y$
<n>=1				113.54	16.49	78.66	113.54	16.49	78.66
<n>=2	1.91	1.22	1.54	1.62	1.65	5.51	10.78	4.42	1.77
<n>=3	14.76	6.2		1.44			0.111	0.11	0.24
<n>=4	7.12	3.5	0.13	1.27		2.38	0.014	0.009	0.008
<n>=5	26.1	13.4		0.2		0.11	0.009		0.007
<n>=6	18.52	13.02		0.056		1.11			

Table S3 Rashba splitting energies for PEA_2PbI_4 and $PEA_2MAPb_2I_7$, calculated with PBE and HSE06 functional.

	PBE			HSE06		
Material Structure	**$E_{R,\ Electron}$ (meV)**	**$E_{R,\ Hole}$ (meV)**	**E_g (eV)**	**$E_{R,\ Electron}$ (meV)**	**$E_{R,\ Hole}$ (meV)**	**E_g (eV)**
PEA_2PbI_4	131.69	10.98	1.457	138.08	9.87	1.970
$PEA_2MAPb_2I_7$	8.09	0.24	1.027	6.40	0.14	1.532

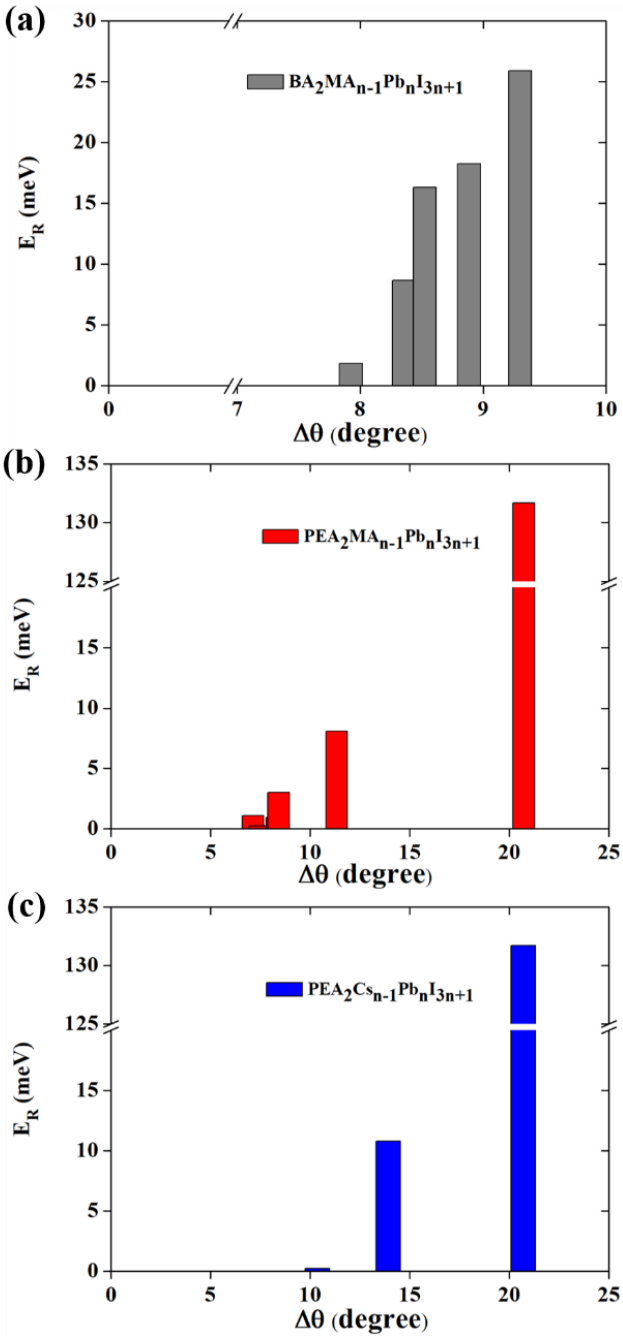

Fig. S1: The correlation between the splitting energy at the conduction band and the average distortion of the octahedrons in (a)$(BA)_2MA_{n-1}Pb_nI_{3n+1}$, (b)$(PEA)_2MA_{n-1}Pb_nI_{3n+1}$ and (c)$(PEA)_2Cs_{n-1}Pb_nI_{3n+1}$ (<n>=1~6) (Upon Cs substitution, the lattice

parameters as well as all atomic positions were relaxed.)

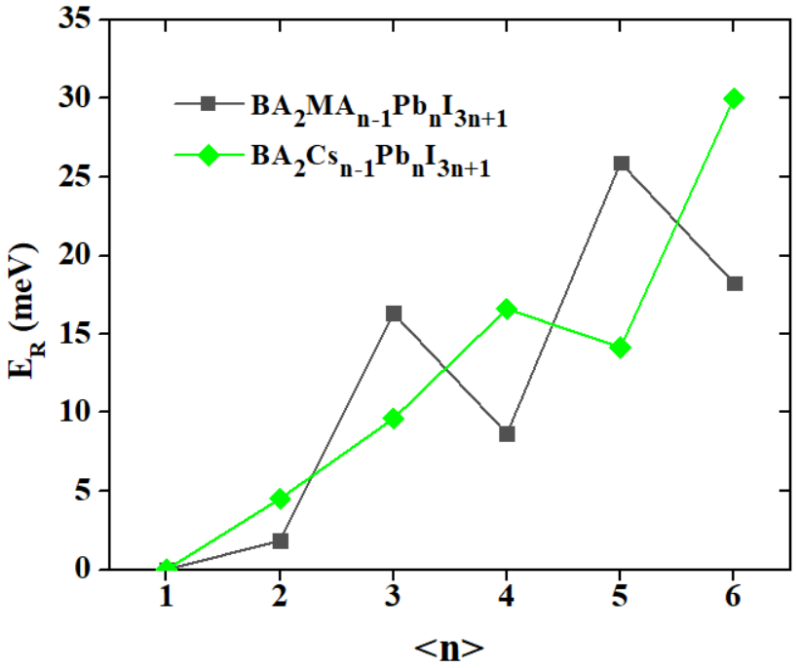

Fig. S2 Calculated Rashba splitting energies for $(BA)_2MA_{n-1}Pb_nI_{3n+1}$, and $(BA)_2Cs_{n-1}Pb_nI_{3n+1}$ (<n>=1~6) at the conduction band edge. (Upon Cs substitution, only positions of Cs cations were relaxed, the lattice parameters and all other atomic positions were fixed.)

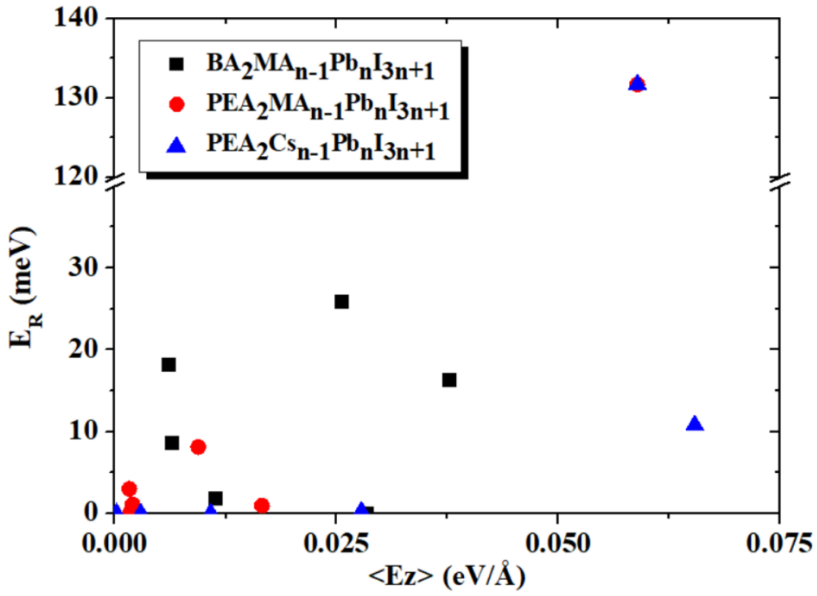

Fig. S3 The correlation between the splitting energy at the conduction band and the average electric field E_Z in each inorganic layer in $(BA)_2MA_{n-1}Pb_nI_{3n+1}$, $(PEA)_2MA_{n-1}Pb_nI_{3n+1}$ and $(PEA)_2Cs_{n-1}Pb_nI_{3n+1}$ (<n>=1~6) (Upon Cs substitution, the lattice parameters as well as all atomic positions were relaxed.)